Light-induced nonequilibrium response of the superconducting cuprate La$_{2-x}$Sr$_x$CuO$_4$

Hiroaki Niwa,[1] Naotaka Yoshikawa,[1] Kaito Tomari,[1] Ryusuke Matsunaga,[2]
Dongjoon Song,[3] Hiroshi Eisaki,[3] and Ryo Shimano[1,4]

[1]*Department of Physics, The University of Tokyo, Hongo, Tokyo 113-0033, Japan*
[2]*Laser and Synchrotron Research Center, The Institute for Solid State Physics, The University of Tokyo,*
5-1-5 Kashiwanoha, Kashiwa, Chiba 277-8581, Japan
[3]*National Institute of Advanced Industrial Science and Technology, Tsukuba 305-8568, Japan*
[4]*Cryogenic Research Center, The University of Tokyo, Yayoi, Tokyo 113-0032, Japan*

We report the dynamics of the cuprate superconductor La$_{2-x}$Sr$_x$CuO$_4$ ($x = 0.14$) after intense photoexcitation utilizing near-infrared (800 nm) optical pump-terahertz probe spectroscopy. In the superconducting state at 5 K, we observed a redshift of the Josephson plasma resonance that sustains for hundreds of picoseconds after the photoexcitation, indicating the destruction of the c-axis superconducting coherence. We show that the metastable spectral features can be described by the photoinduced surface heating of the sample. We also demonstrate that the conventional analysis used to extract the spectra of the photoexcited surface region can give rise to artifacts in the nonequilibrium response.

I. INTRODUCTION

In unconventional high-temperature superconductors, it has been revealed that various electronic states emerge depending on temperature and chemical doping, such as the antiferromagnetic insulator, spin density wave, stripe order, charge order, pair density wave, nematic order, and pseudogap [1]. It is now commonly recognized that the elucidation of the interplay of those multiple orders as well as the unveiling of pairing glue is crucial to understanding the emergence of superconductivity. In these aspects, the study of real-time dynamics of superconductivity by ultrafast spectroscopy technique has been playing important roles [2–4]. For instance, ultrafast pump-probe experiments have shown their ability to elucidate bosonic fluctuations to which fermionic quasiparticles couple. The time-resolved observation of collective modes enables the direct access to the order parameter dynamics in nonequilibrium [5–7], and for cuprate superconductors it has been used to reveal the coupling between the superconductivity and the charge density wave order [8,9].

Searching for a new state of matter induced by the photoexcitation is also a fascinating subject in this respect, as it provides deeper insight into the competing orders or hidden states, with revealing new functionalities of correlated materials. Light-induced superconductivity is a highly intriguing example, where the strong photoexcitation leads to a transient emergence of a superconductivity-like response above the critical temperature T_c [10–15]. For example, in La$_{2-x}$Ba$_x$CuO$_4$, the transient reappearance of Josephson plasma resonance (JPR), one of the characteristic fingerprints of superconductivity, has been observed in the c-axis terahertz (THz) response above T_c right after intense near-infrared photoexcitation [13,14]. It has been suggested that the photoexcitation suppresses the competing stripe charge order [13,14,16], although the microscopic origin of this light-induced phenomenon remains to be resolved. The

photoexcited state of La$_{2-x}$Ba$_x$CuO$_4$ below T_c is even more unclear. Though a transient enhancement of the JPR frequency was primarily reported [13], recent experimental results have suggested an existence of a photoinduced metastable phase, where a new JPR mode and significant increase of spectral weight in optical conductivity are observed [17,18]. Hence, the role of intense photoexcitation and its relation with the preexisting competing orders remain to be clarified.

Here, we investigate the photoexcited dynamics in the nearly optimal-doped La$_{2-x}$Sr$_x$CuO$_4$ ($x = 0.14$), one of the archetypal cuprate superconductors, by utilizing near-infrared optical-pump and THz-probe spectroscopy. In La$_{2-x}$Sr$_x$CuO$_4$, the effect of charge stripe order has been reported to be less pronounced compared to La$_{2-x}$Ba$_x$CuO$_4$ [19,20]. In addition, previous ultrafast pump-probe studies of La$_{2-x}$Sr$_x$CuO$_4$ have presented a destruction of superconductivity after the photoexcitation [21–23]. Thus, La$_{2-x}$Sr$_x$CuO$_4$ provides an interesting platform to expose how the significance of stripe charge order affects the photoexcited state below T_c. With increasing excitation density, the JPR shifts to the low-energy side which sustains for several hundreds of picoseconds, indicating a quasiequilibrium state with suppressed bulk superconducting coherence. We show that this quasiequilibrium state is well explained by the thermalization due to the photoexcitation. At the same time, we argue the breakdown of conventional analysis used in optical pump-THz probe experiments, which is prone to produce nonexistent features in the THz-range spectra.

II. EXPERIMENTS

A. Methods

We used a bulk La$_{2-x}$Sr$_x$CuO$_4$ single crystal with the doping level of $x = 0.14$ grown by the floating-zone method. The mirror-polished ac surface of the sample ($7 \times 7 \times 5$ mm^3)
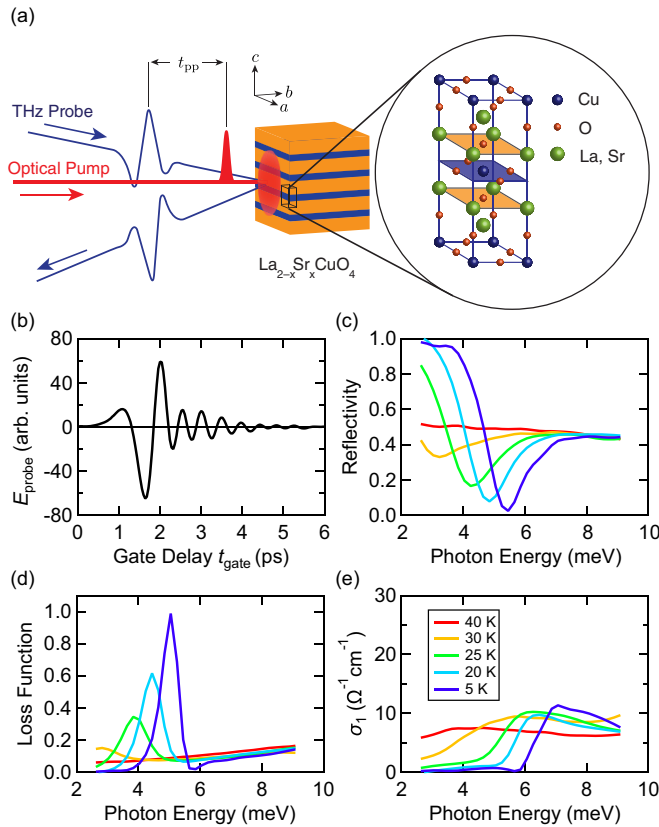
FIG. 1. Experimental setup and optical properties in equilibrium. (a) Schematic of the optical pump-THz probe experiment and the crystal structure of $La_{2-x}Sr_xCuO_4$. Both pump and probe pulses are polarized along the c-axis direction of the crystal. (b) Time-domain waveform of the probe THz pulse generated from ZnTe. (c)–(e) Reflectivity, loss function and real-part optical conductivity of $La_{2-x}Sr_xCuO_4$ ($x = 0.14$) from 5 to 40 K, respectively.

was used and masked by a metal plate with a tapered 4-mm hole. A gold mirror was also mounted on the sample holder as a reference for the reflectivity measurement by THz time-domain spectroscopy (THz-TDS). In Fig. 1(a) we show a schematic of near-infrared optical pump-THz probe spectroscopy. As a light source we used a Ti:Sapphire-based regenerative amplifier with the pulse energy of 4.2 mJ, repetition rate of 1 kHz, pulse duration of 100 fs, and center wavelength of 800 nm. The output of the laser was divided into three beams; each for the optical pump, the generation of the THz probe, and the gate pulse for the THz-TDS, respectively. The optical pump beam has a Gaussian profile with $1/e^2$ diameter of 9 mm, which ensures spatial uniformity of excitation density on the probed region. The THz pulse was generated by the optical rectification in a large-aperture ZnTe crystal and linearly polarized along the c-axis of $La_{2-x}Sr_xCuO_4$. The reflected THz pulse was detected by the electro-optic sampling in a ZnTe crystal with the gate pulse. The waveform of the probe THz pulse is shown in Fig. 1(b). For the evaluation of equilibrium spectral properties, we blocked the path of optical pump and measured the THz waveform reflected from the sample and the reference. For optical pump-THz probe spectroscopy, we utilized two optical

choppers and limited the pump arrival to once in every 10 ms to avoid the average heating effect, and measured the THz waveform with optical pump and without pump simultaneously (see Appendix A for more details).

B. Equilibrium properties

Figures 1(c) to 1(e) show the optical properties of $La_{2-x}Sr_xCuO_4$ ($x = 0.14$) in equilibrium. In the reflectivity spectrum [Fig. 1(c)], a sharp plasma edge associated with the JPR is discerned below T_c. Concomitantly, the loss function spectrum [Fig. 1(d)] as defined by $-\mathrm{Im}(1/\varepsilon(\omega))$ with $\varepsilon(\omega)$ the complex dielectric function exhibits a single peak, corresponding to the longitudinal JPR mode. As temperature decreases the plasma edge shows a blueshift and approaches to 5.5 meV reflecting the development of c-axis superconducting coherence, which is in good agreement with the previous studies [24–27]. A notable feature is identified in the c-axis real-part optical conductivity $\sigma_1(\omega) = \mathrm{Re}[\sigma(\omega)]$ as shown in Fig. 1(e); the low-frequency spectral weight is gradually suppressed below T_c and exhibits gap-like behavior at the lowest temperature. This spectral feature has also been identified in previous reports on the c-axis optical response of $La_{2-x}Sr_xCuO_4$ [24,26,27]. As the origin of this spectral peak in $\sigma_1(\omega)$, two scenarios have been considered: (1) the transverse Josephson plasma mode activated by inhomogeneous distribution of interlayer Josephson coupling constant [28,29], and (2) the in-plane inhomogeneity of superconductivity associated with the spin-density wave [26,27], while its assignment remains an open issue.

III. RESULTS OF PHOTOEXCITED STATE

Now we show the result of near-infrared optical pump-THz probe spectroscopy of $La_{2-x}Sr_xCuO_4$ ($x = 0.14$) with the optical pump linearly polarized along the c-axis. We also investigated the pump polarization along the a-axis and obtained similar results (see Appendix B). Figure 2(a) shows transient reflectivity measured at 3 ps after the optical pump ($t_{pp} = 3$ ps). As the pump fluence increases, the JPR plasma edge shows a gradual redshift, indicating the reduction of c-axis superconducting coherence. Figure 2(b) shows the time evolution of transient reflectivity at the photoexcitation density of $1300\,\mu J/cm^2$. The pump-induced redshift of JPR is most significant right after the excitation ($t_{pp} = 3$ ps), and
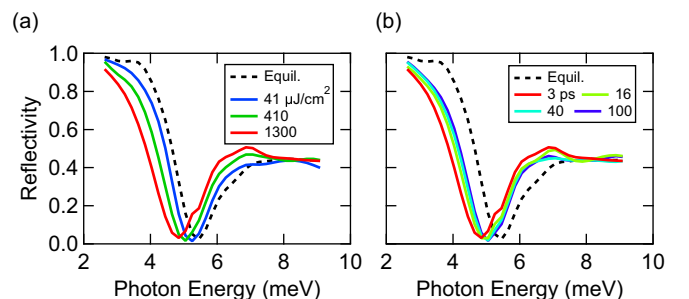

FIG. 2. (a) Pump-fluence dependence of transient reflectivity at $t_{pp} = 3$ ps. (b) Time evolution of transient reflectivity at the pump fluence of $1300\,\mu J/cm^2$.

shows slow recovery toward the equilibrium plasma frequency. The spectral features at $t_{pp} = 40$ ps and $t_{pp} = 100$ ps are almost identical, suggesting that at $t_{pp} = 40$ ps the system has reached quasiequilibrium. A hump structure in reflectivity emerges around 6–7 meV and shows the same relaxation behavior in terms of its timescale.

Here, we compare the nonequilibrium dynamics to previous studies. Ultrafast dynamics of the photoexcited La$_{2-x}$Sr$_x$CuO$_4$ has been studied by transient reflectivity measurements at 800 nm [21–23] and by THz transmittance measurements [23]. In optical pump-probe measurements using a thin-film La$_{2-x}$Sr$_x$CuO$_4$, the excitation density required to destroy the superconductivity at $t_{pp} = 3$ ps has been estimated to be 2.4 K/Cu [23], which corresponds to approximately 30 μJ/cm^2 in our current experimental setup. Therefore, we expect that in our result shown in Fig. 2(a) the superconductivity is destroyed in all three pump fluences at $t_{pp} = 3$ ps. The transient reflectivity in Fig. 2, however, shows only the slight redshift of JPR without complete suppression. It can be ascribed to the penetration-depth mismatch of the pump and probe pulses. The penetration depth of the THz probe is on the order of 10 μm, whereas the penetration depth at 800 nm is around 660 nm as obtained from the literature values [25]. Therefore, in optical pump-THz probe measurements in reflection geometry, what we observe is the mixed response of small contribution from the surface photoexcited region on top of the large contribution from the equilibrium background. The consideration of the penetration-depth mismatch will be discussed in more detail in the later section.

The intense photoexcitation leads to the heating of the sample, which has been a well-known contribution in pump-probe experiments. The pump energy density required to destroy the superconductivity at $t_{pp} = 100$ ps after the photoexcitation, where the electronic system and the lattice system are considered to reach the temperature just above T_c, has been evaluated as 13.7 K/Cu from the saturation behavior of the pump-probe signal [23]. This photoexcitation intensity corresponds to approximately 150 μJ/cm^2, thus for the pump fluence of 410 μJ/cm^2 and above, we expect that photoexcited sample has been heated up above T_c and the superconductivity is thermally destroyed.

IV. ANALYSIS OF THE PHOTOEXCITED STATE

A. Modeling of the quasiequilibrium state

To examine the effect of pump-induced heating in quasiequilibrium state, we consider a following model of spatial distribution of the refractive index $n^{\mathrm{H}}(\omega, z)$, assuming that all of the injected energy by photoexcitation is converted to the temperature increase at the surface region of the sample. Utilizing the result of specific heat measurement [30], one can convert the pump-energy density to the amount of temperature increase at each sample depth z (see Appendix D for the details of calculation.). In Fig. 3(a), we show the fluence of the optical pump $F_{pump}(z)$ for 1300 μJ/cm^2 excitation and corresponding quasiequilibrium temperature $T_{samp}(z)$ obtained by converting the pump-energy density to the local temperature. Quite remarkably, we see that the photoexcitation affects the sample temperature much more deeply into the sample by an
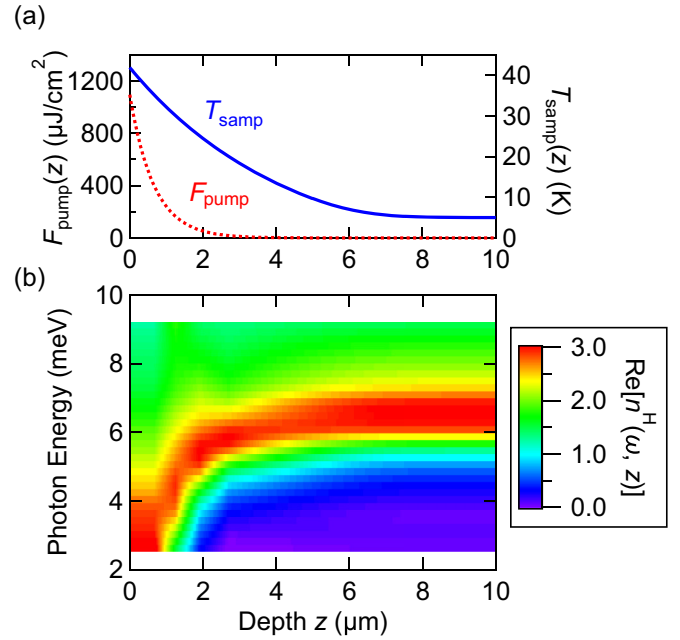

FIG. 3. Simulation of the sample heating induced by the optical excitation. (a) Pump fluence $F_{pump}(z)$ at 1300 μJ/cm^2 excitation (red dotted line) and the corresponding temperature $T_{samp}(z)$ (blue solid line) at the sample depth z. (b) Constructed spatial distribution of the real-part refractive index Re[$n^{\mathrm{H}}(\omega, z)$].

order of magnitude compared to the pump penetration depth; $F_{pump}(z)$ shows an exponential decay in the length scale of the pump penetration depth, but $T_{samp}(z)$ slowly recovers back to its original equilibrium temperature in 6 μm. The discrepancy can be ascribed to the nonlinear dependence of the specific heat with respect to temperature, and especially due to small electronic specific heat at low temperature.

From the obtained temperature distribution $T_{samp}(z)$, it is now possible to construct $n^{\mathrm{H}}(\omega, z)$ by assigning equilibrium data of the refractive index at the corresponding temperature for each z, which is presented in Fig. 3(b). The total response of the sample with $n^{\mathrm{H}}(\omega, z)$ when observed by the THz pulse can be obtained as the effective refractive index $n^{\mathrm{H}}_{eff}(\omega)$, by assuming the surface region of the sample as a stack of thin layers and calculating the Fresnel coefficients considering the multiple reflections (see Appendix E for the details of the calculation.). In Fig. 4, we compare the experimental results of energy reflectivity and the pump-induced phase shift measured at $t_{pp} = 100$ ps to the calculated energy reflectivity and phase shift from the simulation of $n_{eff}(\omega)$ for various pump fluences. Here, we define the pump-induced phase shift $\theta(\omega)$ as $\theta(\omega) = \arg(r_{wp}(\omega)/r_{np}(\omega))$, where $r_{wp}(\omega)$ ($r_{np}(\omega)$) is the complex reflectivity measured with (without) optical pump. We see that the simulation result describes the behavior of both the amplitude and the phase observed in the quasiequilibrium state consistently. The growth of the hump structure around 6–7 meV in energy reflectivity is also apparent in the simulation. The phase shift shows a pronounced decrease near the equilibrium JPR frequency, which can be ascribed to the suppression of JPR in quasiequilibrium state. At earlier pump-probe delay time, application of the heating simulation may
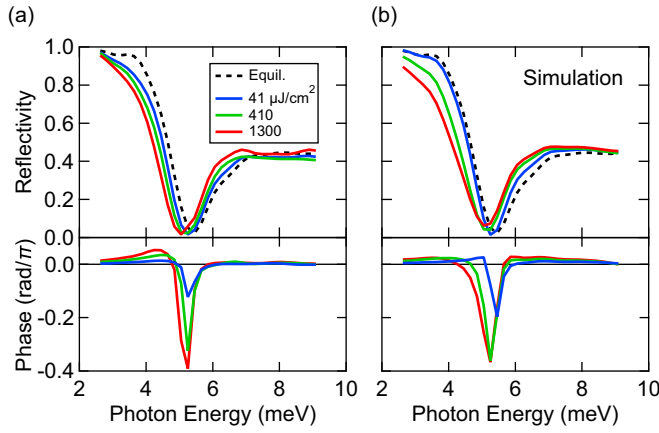
FIG. 4. Comparison of the experimental result to the heating simulation. (a) Pump-fluence dependence of energy reflectivity and pump-induced phase shift measured at $t_{pp} = 100$ ps and (b) corresponding results obtained from the heating simulation.

not be appropriate because the sample is in the middle of the thermalization processes to reach the quasiequilibrium state and the sample temperature cannot be clearly defined. In addition, ballistic thermal transport may modify the spatial profile of the temperature gradient. Nevertheless, the spectral features in the quasiequilibrium state in photoexcited $La_{2-x}Sr_xCuO_4$ observed at longer delay time can be understood by considering the sample heating due to the energy injection by the optical pump.

B. Possible artifacts produced in conventional pump-probe analysis

To gain further insight toward the spectra in the photoexcited state, we must consider the penetration-depth mismatch between the pump and probe to obtain the response functions such as the loss function and optical conductivity. In previous studies of optical pump-THz probe experiments in reflection geometry, this discrepancy was taken into account by postulating a function form for the spatial distribution of complex refractive index $n(\omega, z)$. One example is the multilayer analysis [11,17], where one assumes that the photoinduced change of the spatial profile of the complex refractive index $n^{ML}(\omega, z)$ can be written by the exponential decay with respect to the pump penetration depth d_{pump}, i.e.,

$$n^{ML}(\omega, z) = n_{eq}(\omega) + (n_{surf}(\omega) - n_{eq}(\omega))e^{-z/d_{pump}}, \quad (1)$$

where $n_{eq}(\omega)$ and $n_{surf}(\omega)$ are the equilibrium and photoexcited surface complex refractive index, respectively. One can then calculate the effective refractive index $n_{eff}^{ML}(\omega)$, which is determined in the same manner as the heating simulation of quasiequilibrium state in Sec. IV A, and obtain the value of $n_{surf}(\omega)$ such that $n_{eff}^{ML}(\omega)$ fits the complex refractive index obtained from experiments. Another method is the single-layer analysis [12–14,18], where one assumes that the photoexcitation creates a thin nonequilibrium layer at the surface with the thickness of d_{pump} on top of the equilibrium bulk, and includes all of the photoinduced effects into the surface thin
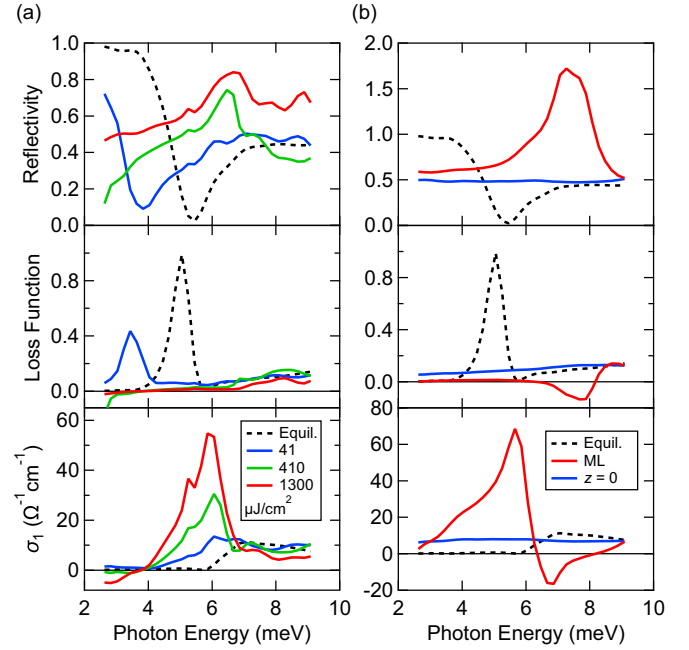

FIG. 5. (a) Pump-fluence dependence of reflectivity, loss function, and real-part optical conductivity at $t_{pp} = 100$ ps extracted after the multilayer analysis. (b) Reflectivity, loss function, and real-part optical conductivity obtained from the multilayer analysis of $n_{eff}^H(\omega)$ for $1300\,\mu J/cm^2$ excitation shown in Figs. 4(b) (red), and corresponding spectra calculated from $n^H(\omega, z = 0)$ of the heating simulation (blue).

layer, i.e.,

$$n^{SL}(\omega, z) = \begin{cases} n_{surf}(\omega), & (z \leqslant d_{pump}), \\ n_{eq}(\omega), & (\text{otherwise}). \end{cases} \quad (2)$$

As far as the extraction of $n_{surf}(\omega)$ is concerned, both procedures are known to produce similar spectral features at the sample surface [13,14,17]. Here, we applied the former multilayer analysis and reconstructed the transient optical spectra at the photoexcited sample surface based on the obtained $n_{surf}(\omega)$.

In Fig. 5(a), we present the fluence dependence of the energy reflectivity, loss function and real-part optical conductivity at $t_{pp} = 100$ ps after extracting the surface refractive index by applying the multilayer analysis to the experimental result shown in Fig. 4(a). The superconducting JPR shows a strong redshift even in the weak excitation regime ($41\,\mu J/cm^2$), and it is completely suppressed for stronger excitation density. In the real-part conductivity, a sharp peak emerges from the edge of the conductivity gap and evolves into a prominent peak with increasing pump fluence.

However, as we demonstrated in Sec. IV A and Fig. 4(b), the nonequilibrium optical spectra are reproduced by taking into account the pump-induced heating effect. Supposing the effective refractive index from the heating simulation $n_{eff}^H(\omega)$ as an experimental result and applying the multilayer analysis, we can now compare the extracted photoexcited surface spectra obtained from $n_{surf}(\omega)$ with the spectra at $z = 0$ of the heating simulation, which can be calculated using $n^H(\omega, z = 0)$. We show the comparison of the extracted surface spectra and

the simulated data for $1300\,\mu J/cm^2$ excitation in Fig. 5(b). The spectra calculated from $n_{surf}(\omega)$ of the simulation result also present the similar behavior of increased energy reflectivity and corresponding increase in spectral weight in the real-part optical conductivity. The effect is more exaggerated in the simulated spectra particularly for the reflectivity and the loss function between 7 to 8 meV. These exaggerations may be caused by the nonlinear effect in energy absorption by the pump pulses that is not included in our heating simulation, or accumulation of phase-sensitive errors in the procedure which becomes pronounced especially in higher frequencies. On the other hand, the actual surface spectra obtained from $n^H(\omega, z = 0)$ of the heating simulation show featureless reflectivity, loss function, and optical conductivity. This comparison demonstrates a possibility that the conventional method to extract the surface response functions does not provide the actual spectra at the surface but instead resulting in artificial spectral properties.

The observation of artifacts presented in Fig. 5 directly points out the fragility of surface reconstruction methods. As we can clearly see in Fig. 3, the spatial distribution of refractive index does not follow the exponential decay. The validity of the function form of $n(\omega, z)$, both in single-layer and multilayer analysis, may break down and lead to artifacts especially under the high-intensity photoexcitation. In such a case, the acquisition of the actual form of $n(\omega, z)$ becomes crucial, but its analytical determination is a challenging task. Also, in the multilayer analysis we assume that the photoexcitation affects the spectral properties only within the pump penetration depth of the sample. However, the heating simulation suggests that the effect of photoexcitation in terms of the rise in temperature affects much deeper into the sample than the penetration depth [see, e.g., Fig. 3(a)]. To examine the photoexcited state more accurately in bulk samples, the pump-probe penetration depth mismatch should be resolved carefully.

Before concluding, it is worth mentioning again that the modeling of the sample heating in this study is not fully applicable in the timescale within the relaxation time where the system has not reached quasithermal equilibrium. Indeed, in our result at 3 ps [Fig. 2(a)], we observed a difference between the experimental result and the simulation. In addition, since the specific heat of phonons becomes significantly larger with increasing temperature, the effect of pump-induced temperature increase should be infinitesimal in higher equilibrium temperature, including the measurements performed above T_c, and cannot account for the emergence of JPR-like structure above T_c as observed in the stripe-phase $La_{2-x}Ba_xCuO_4$ [13,14]. Furthermore, our result of the photoexcitation of $La_{2-x}Sr_xCuO_4$ ($x = 0.14$) right at $T_c = 35$ K does not present any photoinduced change in the reflectivity spectra (see Appendix C), showing a stark contrast with the observation in the stripe-phase $La_{2-x}Ba_xCuO_4$ and suggesting a possibility that the presence of competing stripe order plays an essential role in the photoexcited state.

V. SUMMARY

We investigate the photoexcited nonequilibrium response of the high-T_c cuprate superconductor $La_{2-x}Sr_xCuO_4$ ($x =$ 0.14) by utilizing near-infrared optical pump-THz probe spectroscopy. In the superconducting state, the continuous redshift of JPR was observed with increasing the photoexcitation density, indicating the destruction of superconductivity. We demonstrate that the quasiequilibrium spectral feature appearing after photoexcitation is reproduced considering the sample surface heating induced by the pump energy. We also point out that conventional pump-probe analysis to extract the response function of photoexcited sample surface in optical pump-THz probe experiments can present serious artifacts in the transient spectra.

APPENDIX A: DETAILS OF THE DATA ACQUISITION AND ANALYSIS IN THE PUMP-PROBE MEASUREMENT

The pump-induced change of the photoexcited signal at the pump-probe delay time t_{pp} was obtained by utilizing the optical chopper to measure simultaneously the time-domain signal with the optical pump $E_{wp}(t; t_{pp})$ and without pump $E_{np}(t; t_{pp})$. By performing Fourier transform we obtained complex spectra $E_{wp}(\omega; t_{pp})$ and $E_{np}(\omega; t_{pp})$. We calculated the nonequilibrium complex reflectivity $r_{pp}(\omega; t_{pp})$ by multiplying the pump-induced change to the equilibrium complex reflectivity $r_{eq}(\omega)$,

$$r_{pp}(\omega; t_{pp}) = \frac{E_{wp}(\omega; t_{pp})}{E_{np}(\omega; t_{pp})} r_{eq}(\omega). \tag{A1}$$

Using $r_{pp}(\omega; t_{pp})$, we obtained the transient reflectivity $R_{pp}(\omega; t_{pp}) = |r_{pp}(\omega; t_{pp})|^2$, which are presented in Figs. 2, 4(a), 7(a), and 8.

The key assumption in Eq. (A1) is that the spectral feature of $E_{np}(\omega; t_{pp})$ is identical to the spectrum measured in equilibrium state $E_{eq}(\omega)$. However, if the modulation frequency of optical chopper for the optical pump is too fast under high pump fluence, the sample presents accumulative temperature increase because the next optical pump arrives at the sample before the sample temperature recovers back to its original equilibrium temperature. In such a case, the identity between $E_{np}(\omega; t_{pp})$ and $E_{eq}(\omega)$ is violated. To avoid this average heating effect, we used two optical choppers with the modulation frequency of 100 Hz to limit the pump arrival to once in every 10 ms, as we illustrate in Fig. 6.

APPENDIX B: PUMP-POLARIZATION DEPENDENCE OF THE PHOTOEXCITED STATE

We discuss briefly the pump-polarization dependence of the photoexcited state. In Fig. 7(a), we show the result of a-axis and c-axis photoexcitation in 5 K measured at $t_{pp} = 3$ ps with the fluence of $1300\,\mu J/cm^2$. For both pump polarization, we observe a similar behavior in the transient reflectivity where it shows a redshift of the JPR plasma edge. Also, we notice that the amount of redshift for the a-axis photoexcitation is smaller compared to the c-axis photoexcitation.
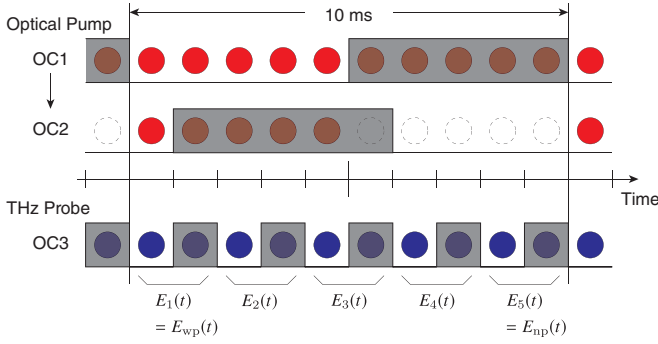
FIG. 6. Schematic of the configuration of optical chopper for the optical pump and THz probe pulses used during the pump-probe measurement. The red and blue circles represent the output of the laser for the optical pump and the probe THz-pulse generation, respectively. The arrival of the optical pump is limited to once in 10 ms by choosing appropriate phases for two optical choppers running at 100 Hz (OC1 and OC2). For the measurement of THz time-domain waveform, we use another optical chopper with the frequency of 500 Hz to obtain $E_{\mathrm{wp}}(t; t_{\mathrm{pp}})$ and $E_{\mathrm{np}}(t; t_{\mathrm{pp}})$ simultaneously.

Here, we argue that this trend can also be understood by making the use of our model of heating simulation. For c-axis photoexcitation, the pump-penetration depth is estimated to be 660 nm as we discussed in Sec. III. By making the use of the values for the a-axis [31], we can estimate the pump-penetration depth of a-axis polarization to be 170 nm, which is about a fourth of the c-axis penetration depth. Then, we expect that the pump-induced effect is confined closer into the surface region of the sample, and thus probing much larger equilibrium region and leading to overall smaller pump-induced change when we look at the transient reflectivity spectrum.

To confirm this picture, we performed the same heating simulation using the a-axis penetration depth. The comparison of the result of the simulation with the c-axis pump-polarization is shown in Fig. 7(b). We see that the simulation shows consistent behavior with the experiment. Although we present the experimental data at $t_{\mathrm{pp}} = 3$ ps, based on the relaxation behavior we expect that this trend is also consistent in the quasiequilibrium state, e.g., $t_{\mathrm{pp}} = 100$ ps.
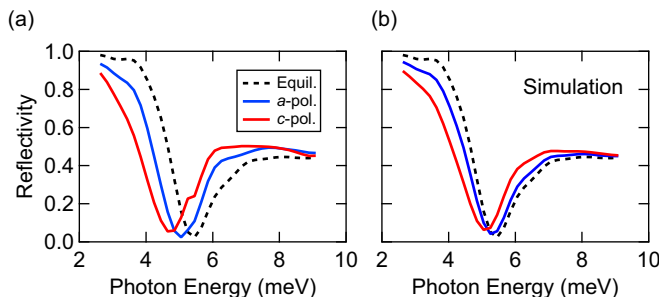

FIG. 7. (a) Transient reflectivity spectra of a-axis and c-axis photoexcitation measured at $t_{\mathrm{pp}} = 3$ ps for 1300 μJ/cm^2 excitation and (b) corresponding results of heating simulation.
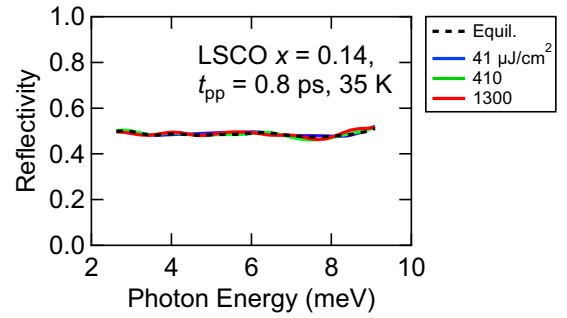

FIG. 8. Pump-fluence dependence of the transient reflectivity measured at 35 K, 0.8 ps after photoexcitation.

APPENDIX C: RESULT OF THE PHOTOEXCITED STATE AT $T = T_{\mathrm{c}} = 35$ K

Studying the behavior of photoexcited state above T_{c} is an intriguing subject with respect to the light-induced superconductivity is gaining more interest recently [10–15]. In our current study of La$_{2-x}$Sr$_x$CuO$_4$, we also performed the measurement right at $T_{\mathrm{c}} = 35$ K, where no equilibrium JPR is apparent. In Fig. 8, we show the pump-fluence dependence of transient reflectivity measured at $t_{\mathrm{pp}} = 0.8$ ps. Even right after the photoexcitation where we expect the largest pump-induced effect, the transient reflectivity does not present any significant change within our detection threshold, presenting a distinct difference with the reports of photoexcited THz response in other cuprate superconductors with competing stripe order.

APPENDIX D: DETAILS OF THE HEATING SIMULATION

We discuss the procedure of simulation to account for the surface heating of the sample in detail. For this simulation, we consider that all of the energy injected by the intense optical excitation contributes to the sample heating in the quasi-equilibrium state. The energy density of the optical pump $I(z)$ can be related with the excitation fluence by assuming an exponential decay by

$$I(z) = (1 - R)\left(-\frac{dF_{\mathrm{pump}}(z)}{dz}\right) = (1 - R)\frac{F_0}{d_{\mathrm{pump}}}e^{-z/d_{\mathrm{pump}}},$$
$$\text{(D1)}$$

where F_0 is the pump fluence, $d_{\mathrm{pump}} \approx 660$ nm is the penetration depth of the optical pump at 800 nm calculated from the literature values [25], and $R \approx 0.15$ is the reflectivity at 800 nm [25]. The absorbed energy $I(z)$ and the temperature increase can be related by utilizing specific heat, which can be described as

$$C(T) = \gamma_0 T + \alpha T^2 + \beta T^3 + \delta T^5, \qquad \text{(D2)}$$

where $\gamma_0 T$ is the electronic specific heat, αT^2 is the specific heat arising from the d-wave superconductivity, $\beta T^3 + \delta T^5$ is the lattice specific heat including the contributions up to T^5 term, respectively. We used the following specific heat coefficients $\gamma_0 = 1.90$ mJ/(molK^2), $\alpha = 0.177$ mJ/(molK^3), $\beta = 0.120$ mJ/(molK^4), and $\delta = 0.00093$ mJ/(molK^6), respectively, which are taken from the fitting result of the

equilibrium specific measurement of the very near doping of $La_{2-x}Sr_xCuO_4$ ($x = 0.15$) [30]. The quasiequilibrium temperature $T_{samp}(z)$ can now be related to $I(z)$ through the following integral equation:

$$I(z) = \int_{T_{eq}}^{T_{samp}(z)} C(T') \, dT', \tag{D3}$$

where T_{eq} is the equilibrium temperature. By numerically solving Eq. (D3), we obtained $T_{samp}(z)$ for various F_0. The construction of spatial distribution of complex refractive index $n(\omega, z)$ was then carried out by assigning equilibrium complex refractive index to each z with corresponding temperature. The temperature-dependent equilibrium complex refractive index was obtained by a linear interpolation of the equilibrium result [Figs. 1(c) to 1(e)] with respect to temperature.

In actual materials, there is also diffusive dynamics that comes into action after photoexcitation. Concerning our model of heating simulation, the main diffusive dynamics to be considered here is the dynamics of phonons, which dominates the heat transport when a temperature gradient exists. The speed of heat transport can be considered to be bounded by the velocity of acoustic phonons. In $La_{2-x}Sr_xCuO_4$, the phonon velocity can be calculated to be $4 \, nm/ps$ at most referring to the previous result of phonon-dispersion measurement and simulation [32], which is also consistent with the discussion provided in previous optical pump-probe spectroscopy [22]. Considering that the actual heat diffusion occurs slower by some factors and the characteristic length scale of thermal gradient reaches to micrometers (see also Fig. 3), the additional effect of diffusion onto our heating simulation model is fractional, and the main spectral features should not be changed significantly by the diffusion. In addition, recent experimental results on the thermal diffusivity of cuprate superconductors reports that the sound velocity is $5.9 \, cm/s = 59 \, nm/\mu s$ [33], and if we refer to this value we expect the effect of heat diffusion should be significantly small.

APPENDIX E: CALCULATION OF THE EFFECTIVE REFRACTIVE INDEX $n_{eff}(\omega)$

Here, we briefly discuss the method to calculate the effective complex refractive index $n_{eff}(\omega)$ from the spatially nonuniform distribution of refractive index along the z-axis $n(\omega, z)$, which has been utilized both in the multilayer analysis and the heating simulation. To numerically solve $n_{eff}(\omega)$, we consider the surface region of the sample as a stack of thin-film layers and calculate the reflectivity coefficients by considering infinite multiple reflections in each thin film, as schematically drawn in Fig. 9. In our current study, we split the sample surface of length $L = 30 \, \mu m$ into $N = 1000$ layers. We denote the thickness of the each thin-film layer as $\Delta L (= L/N)$ and write $n_l(\omega) = n(\omega, l\Delta L)$ to indicate the complex refractive index of the lth layer. When we consider the reflection coefficient of the superconducting bulk to the deepest Nth layer, we use,

$$\bar{r}_{bulk}(\omega) = \frac{n_N(\omega) - n_{eq}(\omega)}{n_N(\omega) + n_{eq}(\omega)}, \tag{E1}$$

where $n_{eq}(\omega)$ is the equilibrium complex refractive index. Now, when we include the Nth layer, the reflected THz probe
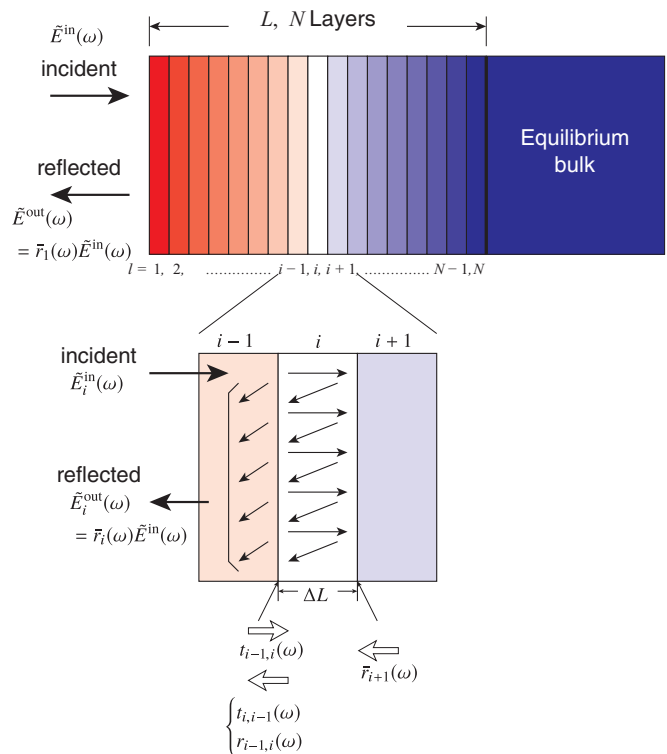

FIG. 9. Schematic of the calculation procedure of the effective complex refractive index $n_{eff}(\omega)$.

acquires the following reflection coefficient:

$$\bar{r}_N(\omega) = r_{N-1,N}(\omega) + t_{N-1,N}(\omega)\bar{r}_{bulk}(\omega)t_{N,N-1}(\omega)e^{i\Phi_N(\omega)}$$

$$\times \sum_{k=0}^{\infty}[r_{N,N-1}(\omega)\bar{r}_{bulk}(\omega)e^{i\Phi_N(\omega)}]^k$$

$$= \frac{r_{N-1,N}(\omega) + \bar{r}_{bulk}(\omega)e^{i\Phi_N(\omega)}}{1 + r_{N-1,N}(\omega)\bar{r}_{bulk}(\omega)e^{i\Phi_N(\omega)}}, \tag{E2}$$

where

$$t_{i,j}(\omega) = \frac{2n_i(\omega)}{n_i(\omega) + n_j(\omega)}, \tag{E3}$$

$$r_{i,j}(\omega) = \frac{n_i(\omega) - n_j(\omega)}{n_i(\omega) + n_j(\omega)} \tag{E4}$$

are the Fresnel coefficients for the transmittance and reflection at the boundary of two layers with $n_i(\omega)$ and $n_j(\omega)$, and $\Phi_i(\omega) = 2n_i(\omega)\omega\Delta L/c$ gives the phase factor of the multiple reflection. Similarly, the effective Fresnel's reflection coefficient at the lth layer $\bar{r}_l(\omega)$ can be calculated using the $\bar{r}_{l+1}(\omega)$,

$$\bar{r}_l(\omega) = \frac{r_{l-1,l}(\omega) + \bar{r}_{l+1}(\omega)e^{i\Phi_l(\omega)}}{1 + r_{l-1,l}(\omega)\bar{r}_{l+1}(\omega)e^{i\Phi_l(\omega)}}. \tag{E5}$$

By repeating this calculation until we reach the surface layer $l = 1$, we can obtain the total effective Fresnel coefficient $\bar{r}_1(\omega)$. For the calculation of $\bar{r}_1(\omega)$, we adopt the refractive index of the sample atmosphere to be $n_{air}(\omega) = n_0(\omega) = 1$. Finally, we can calculate $n_{eff}(\omega)$ as

$$n_{eff}(\omega) = \frac{1 - \bar{r}_1(\omega)}{1 + \bar{r}_1(\omega)}. \tag{E6}$$

[1] For a review, see e.g., B. Keimer, S. A. Kivelson, M. R. Norman, S. Uchida, and J. Zaanen, Nature **518**, 179 (2015).

[2] For a review, see e.g., C. Giannetti, M. Capone, D. Fausti, M. Fabrizio, F. Parmigiani, and D. Mihailovic, Adv. Phys. **65**, 58 (2016).

[3] S. Dal Conte, C. Giannetti, G. Coslovich, F. Cilento, D. Bossini, T. Abebaw, F. Banfi, G. Ferrini, H. Eisaki, M. Greven, A. Damascelli, D. van der Marel, and F. Parmigiani, Science **335**, 1600 (2012).

[4] M. Sentef, A. F. Kemper, B. Moritz, J. K. Freericks, Z.-X. Shen, and T. P. Devereaux, Phys. Rev. X **3**, 041033 (2013).

[5] R. Matsunaga, Y. I. Hamada, K. Makise, Y. Uzawa, H. Terai, Z. Wang, and R. Shimano, Phys. Rev. Lett. **111**, 057002 (2013).

[6] R. Matsunaga, N. Tsuji, H. Fujita, A. Sugioka, K. Makise, Y. Uzawa, H. Terai, Z. Wang, H. Aoki, and R. Shimano, Science **345**, 1145 (2014).

[7] K. Katsumi, N. Tsuji, Y. I. Hamada, R. Matsunaga, J. Schneeloch, R. D. Zhong, G. D. Gu, H. Aoki, Y. Gallais, and R. Shimano, Phys. Rev. Lett. **120**, 117001 (2018).

[8] G. L. Dakovski, W.-S. Lee, D. G. Hawthorn, N. Garner, D. Bonn, W. Hardy, R. Liang, M. C. Hoffmann, and J. J. Turner, Phys. Rev. B **91**, 220506(R) (2015).

[9] J. P. Hinton, E. Thewalt, Z. Alpichshev, F. Mahmood, J. D. Koralek, M. K. Chan, M. J. Veit, C. J. Dorow, N. Barišić, A. F. Kemper, D. A. Bonn, W. N. Hardy, R. Liang, N. Gedik, M. Greven, A. Lanzara, and J. Orenstein, Sci. Rep. **6**, 23610 (2016).

[10] D. Fausti, R. I. Tobey, N. Dean, S. Kaiser, A. Dienst, M. C. Hoffmann, S. Pyon, T. Takayama, H. Takagi, and A. Cavalleri, Science **331**, 189 (2011).

[11] S. Kaiser, C. R. Hunt, D. Nicoletti, W. Hu, I. Gierz, H. Y. Liu, M. Le Tacon, T. Loew, D. Haug, B. Keimer, and A. Cavalleri, Phys. Rev. B **89**, 184516 (2014).

[12] W. Hu, S. Kaiser, D. Nicoletti, C. R. Hunt, I. Gierz, M. C. Hoffmann, M. Le Tacon, T. Loew, B. Keimer, and A. Cavalleri, Nat. Mater. **13**, 705 (2014).

[13] D. Nicoletti, E. Casandruc, Y. Laplace, V. Khanna, C. R. Hunt, S. Kaiser, S. S. Dhesi, G. D. Gu, J. P. Hill, and A. Cavalleri, Phys. Rev. B **90**, 100503(R) (2014).

[14] E. Casandruc, D. Nicoletti, S. Rajasekaran, Y. Laplace, V. Khanna, G. D. Gu, J. P. Hill, and A. Cavalleri, Phys. Rev. B **91**, 174502 (2015).

[15] D. Nicoletti, D. Fu, O. Mehio, S. Moore, A. S. Disa, G. D. Gu, and A. Cavalleri, Phys. Rev. Lett. **121**, 267003 (2018).

[16] V. Khanna, R. Mankowsky, M. Petrich, H. Bromberger, S. A. Cavill, E. Möhr-Vorobeva, D. Nicoletti, Y. Laplace, G. D. Gu, J. P. Hill, M. Först, A. Cavalleri, and S. S. Dhesi, Phys. Rev. B **93**, 224522 (2016).

[17] S. J. Zhang, Z. X. Wang, L. Y. Shi, T. Lin, M. Y. Zhang, G. D. Gu, T. Dong, and N. L. Wang, Phys. Rev. B **98**, 20506(R) (2018).

[18] K. A. Cremin, J. Zhang, C. C. Homes, G. D. Gu, Z. Sun, M. M. Fogler, A. J. Millis, D. N. Basov, and R. D. Averitt, arXiv:1901.10037.

[19] M. Vojta, Adv. Phys. **58**, 699 (2009).

[20] H.-H. Wu, M. Buchholz, C. Trabant, C. F. Chang, A. C. Komarek, F. Heigl, M. Zimmermann, M. Cwik, F. Nakamura, M. Braden, and C. Schüßler-Langeheine, Nat. Commun. **3**, 1023 (2012).

[21] P. Kusar, J. Demsar, D. Mihailovic, and S. Sugai, Phys. Rev. B **72**, 014544 (2005).

[22] P. Kusar, V. V. Kabanov, S. Sugai, J. Demsar, T. Mertelj, and D. Mihailovic, Phys. Rev. Lett. **101**, 227001 (2008).

[23] M. Beyer, D. Städter, M. Beck, H. Schäfer, V. V. Kabanov, G. Logvenov, I. Bozovic, G. Koren, and J. Demsar, Phys. Rev. B **83**, 214515 (2011).

[24] K. Tamasaku, Y. Nakamura, and S. Uchida, Phys. Rev. Lett. **69**, 1455 (1992).

[25] S. Uchida, K. Tamasaku, and S. Tajima, Phys. Rev. B **53**, 14558 (1996).

[26] D. N. Basov, H. A. Mook, B. Dabrowski, and T. Timusk, Phys. Rev. B **52**, 13141(R) (1995).

[27] S. V. Dordevic, S. Komiya, Y. Ando, and D. N. Basov, Phys. Rev. Lett. **91**, 167401 (2003).

[28] D. van der Marel and A. Tsvetkov, Czech. J. Phys. **46**, 3165 (1996).

[29] M. Grüninger, D. van der Marel, A. A. Tsvetkov, and A. Erb, Phys. Rev. Lett. **84**, 1575 (2000).

[30] H.-H. Wen, Z.-Y. Liu, F. Zhou, J. Xiong, W. Ti, T. Xiang, S. Komiya, X. Sun, and Y. Ando, Phys. Rev. B **70**, 214505 (2004).

[31] S. Uchida, T. Ido, H. Takagi, T. Arima, Y. Tokura, and S. Tajima, Phys. Rev. B **43**, 7942 (1991).

[32] S. L. Chaplot, W. Reichardt, L. Pintschovius, and N. Pyka, Phys. Rev. B **52**, 7230 (1995).

[33] J. Zhang, E. M. Levenson-Falk, B. J. Ramshaw, D. A. Bonn, R. Liang, W. N. Hardy, S. A. Hartnoll, and A. Kapitulnik, Proc. Natl. Acad. Sci. USA **114**, 5378 (2017).